

A Coplanar Waveguide Fed Hexagonal Shape Ultra Wide Band Antenna with WiMAX and WLAN Band Rejection

Tapan MANDAL¹, Santanu DAS²

¹ Dept. of Information Technology, Govt. College of Engineering and Textile Technology, Serampore, Hooghly, India, PIN-712201

² Dept. of Electronics & Tele-Comm. Engineering, Bengal Engineering and Science University, Shibpur, Howrah, India, PIN-711103

tapanmandal20@rediffmail.com, santanumdass@yahoo.com

Abstract. *In this paper, a coplanar waveguide (CPW) fed hexagonal shape planar antenna has been considered for ultra-wide band (UWB). This antenna is then modified to obtain dual band rejection. The Wireless Local Area Network (WLAN) and Wireless Microwave Access (WiMAX) band rejections are realized by symmetrically incorporating a pair of L-shape slots within the ground plane as well as a couple of I-shape stubs inserted on the bottom side of radiating patch. The proposed antenna has stop bands of 5.05–5.92 GHz and 3.19–3.7 GHz while maintaining the wideband performance from 2.88–13.71 GHz with reflection coefficient of ≤ -10 dB. The antenna exhibits satisfactory omni-directional radiation characteristics throughout its operating band. The peak gain varies from 2 dB to 6 dB in the entire UWB frequency regions except at the notch bands. Surface current distributions are used to analyze the effects of the L-slot and I-shape stub. The measured group delay has small variation within the operating band except notch bands and hence the proposed antenna may be suitable for UWB applications.*

Keywords

Hexagonal planar antenna, CPW fed, UWB, WLAN band, WiMAX band.

1. Introduction

Ultra-Wide Band (UWB) technology becomes more and more important owing to many wireless applications such as multimedia communications, sensor networks, ground penetrating radar, medical imaging and precision localization systems. Due to the characteristics like high data transmission rates, high precision ranging, low complexity, easy connection and high security, UWB technology has been used in large consumer devices as laptops, digital cameras, high definition TVs and bio-medical sensors. As an essential part of the UWB system, the UWB antenna should be designed with low profile, low volume, low cost, large bandwidth and good omni directional radiation patterns and constant group delay.

In 2002, the US-Federal Communications Commission (US-FCC) approved the UWB frequency band from 3.1 to 10.6 GHz for commercial communication applications [1]. Since then, considerable research efforts have been paid into UWB communication technology. This type of UWB antenna has been realized by using either microstrip line [2–5] or coplanar waveguide (CPW) [6–10] feeding structure. In particular, CPW fed antennas have many salient features like less radiation loss, less dispersion and easy integration with monolithic microwave integrated circuits (MMIC). Therefore, CPW fed UWB antennas are currently under consideration for numerous applications.

Many of UWB antennas have been offered for various applications in the last decade [6–15]. Planar UWB monopole antennas with rectangular [6], disk [7], [8], elliptical [9], hexagonal [10] and triangular [11] shapes have been reported. The CPW fed hexagonal monopole antennas are found to have -10 dB return loss bandwidth for UWB application [10] with large size structure. A compact hexagonal wide slot antenna with microstrip fed monopole for UWB application has been described [2] but its structure is complex.

However, the existing Wireless Local Area Network (WLAN: IEEE 802.11a) and Wireless Microwave Access (WiMAX: IEEE 802.16) service bands of 5.15–5.825 GHz and 3.3–3.7 GHz are responsible for the performance degradation of UWB system because of the interference. These existing narrow bands may cause interferences with the UWB systems. To prevent this problem, UWB antennas with band rejection characteristic is desirable. In the conventional design, band stop filters are added at the end of the antenna or the devices. Thereby the size of the antenna is increased. Several UWB antennas with band rejection characteristic have been proposed [4–6], [8], [11–15]. For printed monopole antennas, the familiar methods to achieve band-notch function are etching slots on the metallic patch, feeder or the ground plane in different shapes such as C-shape [6], [8], [14], U-shape [4], L-shape [5], [11], [12], I-shape [13] slot etc. However, most of the notch band UWB antennas are formed by etching half wavelength or quarter wavelength slot on radiating patch.

UWB antennas with dual notch bands have been surfaced in [15–21]. The configuration is either in complex [14], [17–19], [21] or large in size [15]. An effective technology is to insert open circuited stubs into the UWB antenna. The band notch performance is achieved by placing parasitic strips in close proximity to the antenna [18–20]. However, most of UWB antennas [2–11], [14] do not have more than single notch band which reveals that potential interference from other narrow band may still exist.

In this paper, a CPW-fed simple hexagonal monopole antenna with WLAN and WiMAX band notch characteristics is proposed. The design initially begins with a regular hexagonal monopole antenna (RHMA). The band rejection characteristics are obtained by incorporating a pair of L-slots on the ground plane away from the radiating patch and I-shape stubs on the other side of the patch. All the simulations in terms of impedance bandwidth, input impedance, gain, efficiency are carried out using Method of Moment based IE3D simulation software [22]. In this paper, all reflection coefficient measurements are taken out with the help of Agilent Technologies Vector Network Analyzer (N5230A).

2. Antenna Configuration

2.1 Prototype Antenna Geometry

Fig. 1 shows the geometry of the prototype antenna. It is printed on a substrate with dielectric constant ϵ_r of 4.4 and height h of 1.59 mm. As shown in Fig. 1, there are three sections which comprise the structure of the antenna: CPW transmission-line, rectangular shape ground plane and hexagonal shape radiating patch. A 50Ω CPW transmission line is designed with a strip width W_f of 4.1 mm. The lower band edge frequency f_l has been determined for UWB using formulas [8], [10] given as

$$f_l = \frac{c}{\lambda} = \frac{7.2}{(H + r + T)} \quad (1)$$

where H is the height of the hexagon and r is the radius of an equivalent cylindrical monopole antenna in cm and T is the gap between ground plane and patch in cm. With reference to configurations in Fig. 1, the dimensions of height H and radius r of the equivalent cylindrical monopole antenna are obtained by equating their areas as follows:

$$r = \frac{3L_p}{4\pi}, \quad (2)$$

$$H = \sqrt{3}L_p. \quad (3)$$

2.2 Band – Notch Antenna Design

In another form (Fig. 2) the RHMA is made on the same substrate with the dimensions same as before. A notch band in the frequency range of 5.15–5.825 GHz is

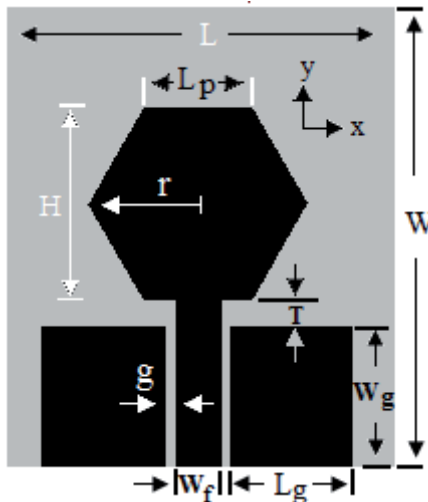


Fig. 1. Geometry of prototype antenna.

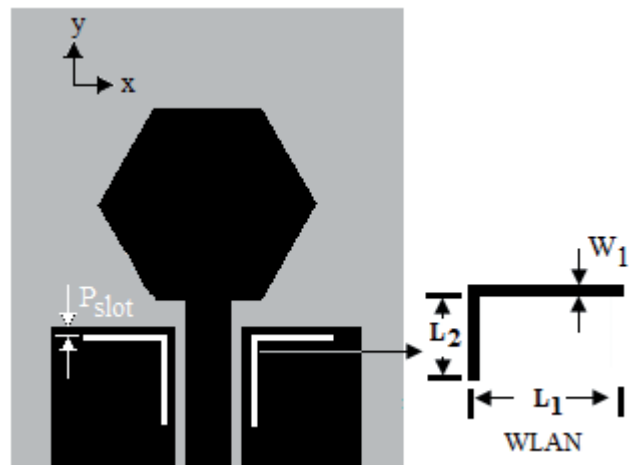


Fig. 2. Geometry of prototype with L-slot antenna.

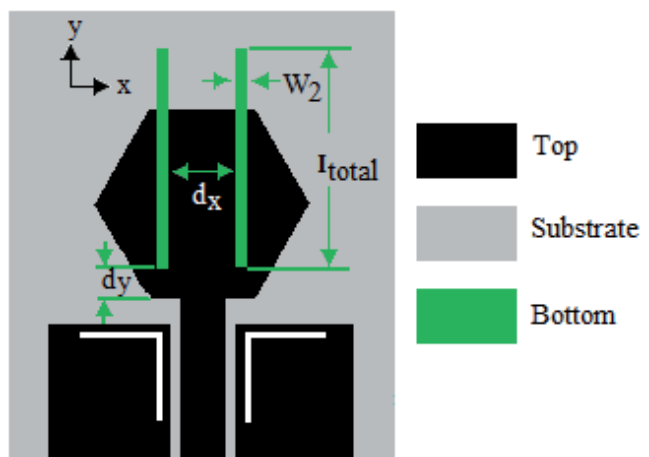


Fig. 3. Geometry of proposed antenna.

obtained by symmetrically inserting a pair of thin L-slots near the feed line within the ground plane. Usually, the length of the each slot is made approximately equal to half the guided wavelength λ_g at the desired notch frequency of the band. This is given by

$$L_{total_WLAN} = \frac{\lambda_g}{2} = \frac{c}{2f_{notch_WLAN} \sqrt{\frac{\epsilon_r + 1}{2}}}, \quad (4)$$

$$L_{total_WLAN} = L_1 + L_2 \quad (5)$$

where L_{total_WLAN} is the length of the slot. For the center notch frequency $f_{notch_WLAN} = 5.5$ GHz the length of the slot is calculated as 16.76 mm. The optimum slot width W_1 is found to be 0.3 mm by way of simulation. In addition to this WiMAX stop band is realized by symmetrically incorporating a couple of narrow I-shape parasitic strips (stubs) on bottom side of the radiating patch (Fig. 3). Each parasitic strip has length of half wavelength at desired notch frequency. For center notch $f_{notch_WiMAX} = 3.5$ GHz, the length of the strip can be determined as 26.13 mm. The optimum strip width W_2 is found to be 1 mm. From (4), (5), the total length of the L-shape slots and I-shape stubs may be obtained at the beginning of the design. Finally the position and lengths are adjusted by using simulator to achieve the desired results.

3. Parametric Study and Observations

In theory, all of the geometrical parameters of Fig. 1 have an effect on the impedance matching. However, some of them may have major effects than others. Specifically, the size of the hexagonal patch, extrusion depth T and ground plane length L_g have considerable effects on the bandwidth. Reflection coefficient characteristics for various radius r of hexagonal patch are shown in Fig. 4. It indicates that as the patch radius increases, the lower edge frequency moves towards the left side of the plot. The main reason is the increase of radius which in turn increases the height H of the monopole antenna. Thus patch plays a significant role for selecting the lower edge frequency of the band. The effects of extrusion depth T on the input impedance are simulated and shown in Fig. 5. From the result, it is observed that T has a strong effect for impedance matching. By optimizing the parameter T , the bandwidth could be improved. The gap creates a capacitance that neutralizes the inductive effects of the radiating patch to produce nearly pure resistive input impedance. The length of the ground plane L_g has important role on matching characteristics over the band of prototype antenna. Fig. 6 shows the effect of varying ground plane length which indicates that the reflection coefficient characteristics is changing significantly while the higher and lower frequency matching is improved. However, at middle of the frequency band, the performance degrades. In this case an optimum value of L_g is taken to be 11.6 mm as a compromise of all frequency matches perfectly. The simulation responses of prototype antenna cover the entire UWB frequency range for $r = 13.6$ mm, $T = 1.375$ mm, $L_g = 11.6$ mm, $g = 0.4$ mm and $W_f = 4.1$ mm.

Next parametric study and discussion are carried out for the antenna with WLAN band rejection (Fig. 2). The

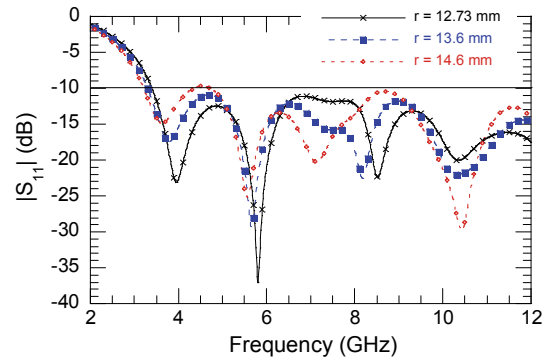


Fig. 4. Simulated reflection coefficient for different radius r .

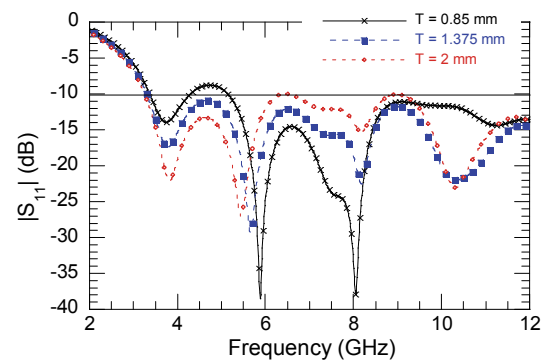


Fig. 5. Simulated reflection coefficient for different T .

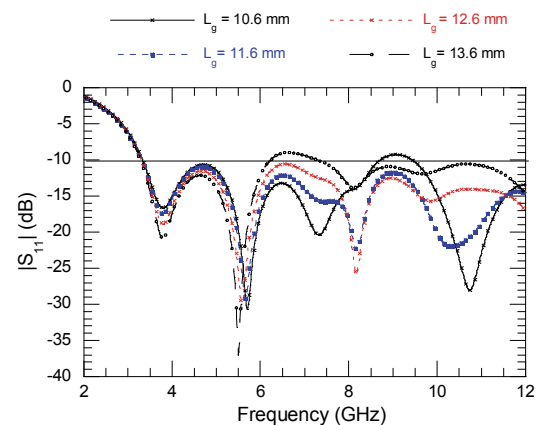


Fig. 6. Simulated reflection coefficient for different L_g .

total length of the inverted L-shape slots etched from the ground plane is deduced as in (4). Two L-shape slots are introduced symmetrically with respect to the fed line of the planar monopole as shown in Fig. 2. A pair of notch frequencies of two slots are coupled together and a band stop characteristics with improved notching and rejection bandwidth is obtained. Here, the reflection coefficient characteristics for various values of slot length L_{total_WLAN} and width W_1 are shown in Fig. 7 to Fig. 8 respectively. Fig. 7 indicates that the notch band moves downwards with higher peak as the length of the L-slots is increased. It is observed from the parametric study that the resonant frequency of the notch-band depends on the length of the slot and notch bandwidth depends upon width of the slot. This property provides a great freedom to the designers to select the notch band for the antennas as is evident from Fig. 7 and Fig. 8.

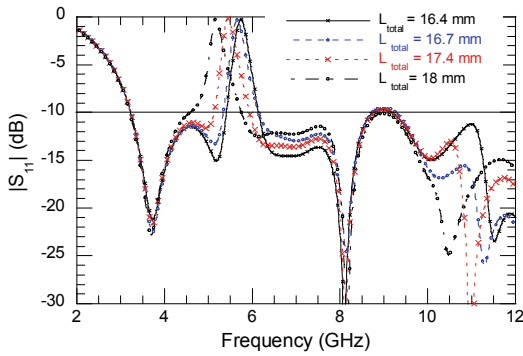


Fig. 7. Reflection coefficient for various lengths of L-slot.

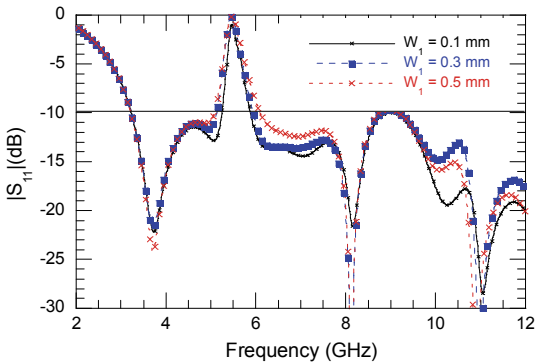


Fig. 8. Reflection coefficient for various width of L-slot.

Fig. 9 shows the reflection coefficient characteristics with changing the position of the slots with other parameters remaining constant. It can be seen that the peak value at notch frequency (5.5 GHz) decreases while the value of P_{slot} rises. An optimum P_{slot} is chosen to be 1 mm by way of parametric study. Due to the presence of L-slots inside the ground plane, maximum current flows back to the feeding part. Therefore, negligible amount of currents radiates from the antenna and degenerates radiation around 5.15 GHz to 5.93 GHz.

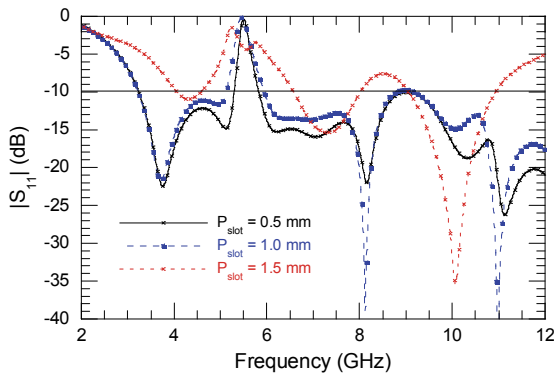


Fig. 9. Effect of position of the L-slots on reflection coefficient.

Furthermore to realize the WiMAX stop band in UWB region, a pair of I-shape strips (stubs) have been incorporated on the other side of substrate. The reflection coefficient plots for various length and width are illustrated in Fig. 10 and Fig. 11 respectively. It is observed from Fig. 10 that the notch band moves downwards with higher

peak as the length of strips is increased. Similarly, it is observed that an increase in width W_2 of resonator results in moving downwards of the center frequency of the notch. Strips length has greater impact than strips width on shifting the frequency as is evident from Fig. 10 and Fig. 11.

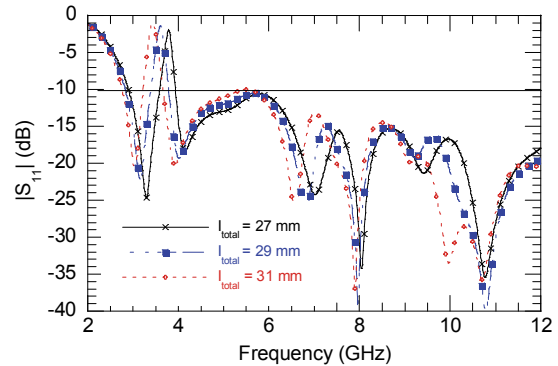


Fig. 10. Reflection coefficient for various length of I-shape stub.

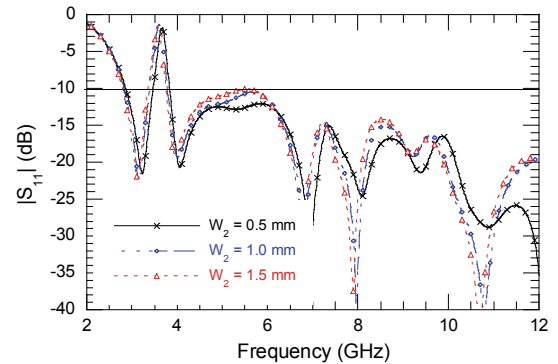


Fig. 11. Reflection coefficient for various width of I-shape stub.

To show the dependency of reflection coefficient on the position of the stub, parametric studies have been done for the same. Fig. 12 and Fig. 13 give the variation in peak value of reflection coefficient with changing the position of the I-strips while other parameters remaining the same. As d_x and d_y value (Fig. 3) rises, the notch BW increases. Therefore, these d_x and d_y have significant freedom for controlling the notch BW. The optimum values of d_x and d_y are chosen to be 11 mm and 3.15 mm respectively. The reflection coefficient characteristics for all the configurations are illustrated in Fig. 14 for a comparison. The detailed design dimensions are given in Tab. 1.

Parameters	L	W	r	H	L_p	L_g
Dimensions	36	48	13.6	23.55	13.6	11.6
Parameters	g	W_f	T	L_1	L_2	W_1
Dimensions	0.4	4.1	1.375	8.4	8.2	0.3
Parameters	L_{total}	W_2	d_x	d_y	P_{slot}	W_g
Dimensions	29	1	11	3.125	1	13.5

Tab. 1. Parameters value of the proposed antenna (dimensions are in mm).

The simulated reflection coefficient characteristics of the proposed antenna reveal stop bands of 0.38 GHz (3.32 to 3.7 GHz) and 0.78 GHz (5.15–5.93 GHz) within the UWB frequency span.

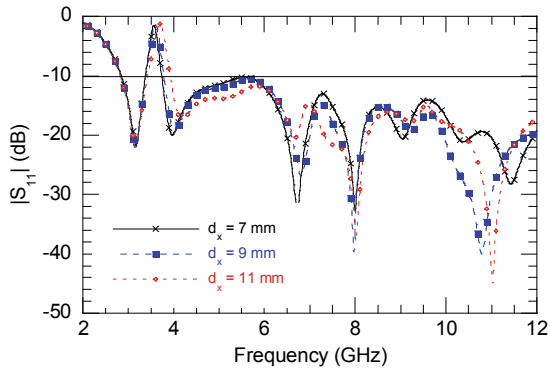


Fig. 12. Simulated reflection coefficient for various value of d_x .

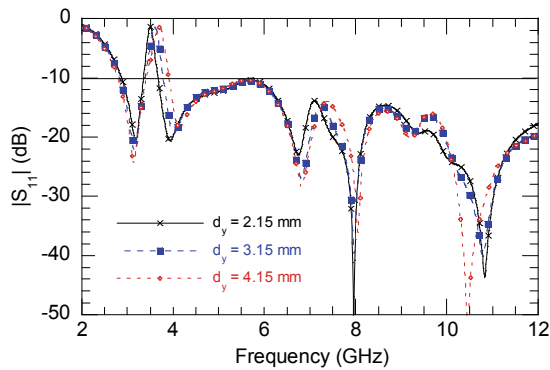


Fig. 13. Simulated reflection coefficient for various value of d_y .

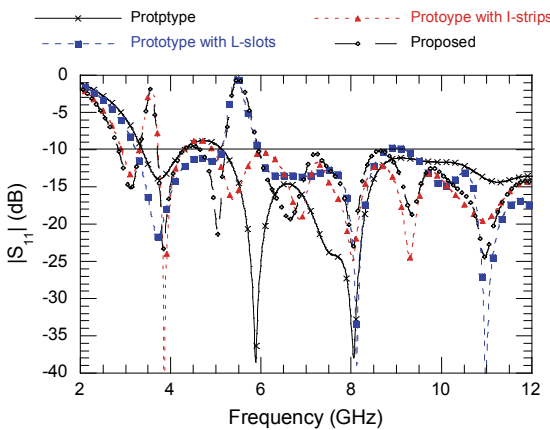


Fig. 14. Reflection coefficient characteristics of all configurations for comparison.

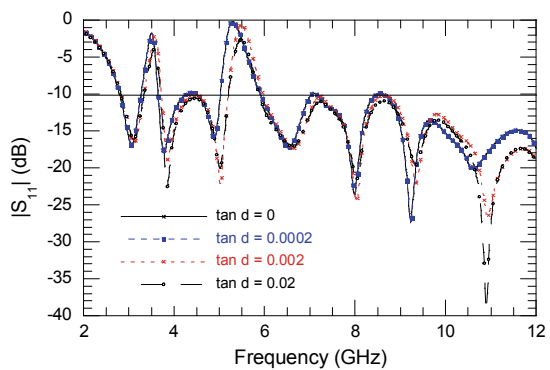


Fig. 15. Reflection coefficient characteristics for various value of loss tangent ($\tan \delta$).

Fig. 15 indicates the reflection coefficient characteristics of the proposed antenna for various values of loss tangent. From the characteristics, it is observed that the peak value of reflection coefficient at notch frequency decreases while the loss tangent of the substrate increases.

4. Experimental Results

Photograph of the prototype and proposed antennas are shown in Fig. 16. The simulated and measured performances of prototype antenna (Fig. 16(a)) are plotted in Fig. 17 for comparison. It is observed from the plot that the simulated response provides BW of 10.37 GHz (3.15 to 13.52 GHz) where the experimental response yields 10.54 GHz (3.06 GHz – 13.60 GHz) impedance band. Therefore, a reasonable good agreement between simulation and measurement is achieved.

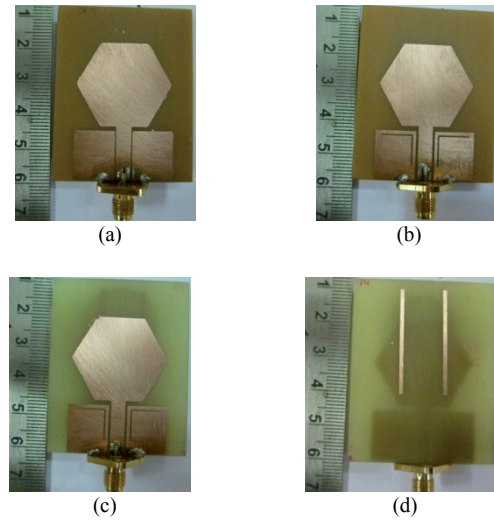


Fig. 16. Photograph of fabricated structure: (a) prototype (top plane), (b) prototype with L-slots (top plane), (c) proposed (top plane), (d) proposed (bottom plane).

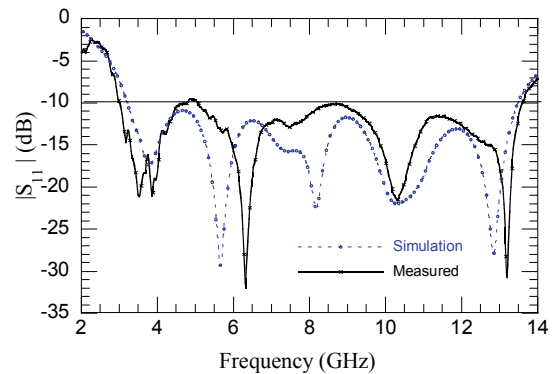


Fig. 17. Comparison between simulation and measured results of the prototype antenna.

Comparison between simulation and measured results of the prototype with L-slots antenna (Fig. 16 (b)) is illustrated in Fig. 18. The simulated reflection coefficient characteristic (Fig. 18) reveals stop band of 0.78 GHz (5.15

to 5.93 GHz) for $S_{11} \leq -10$ dB within the frequency span from 3.15 GHz to 13.08 GHz. The measured characteristic shows 0.86 GHz (5.15–6.01 GHz) stop band which covers the entire WLAN band. The measured result reasonably agrees with the simulated result which has sharp frequency stop band of WLAN band after the L-slots are inserted on the ground plane. The discrepancies between measured and simulated results may be due to the fabrication tolerance of the antenna. The simulated and measured responses of the proposed antenna (Fig. 16(c, d)) are shown in Fig. 19. The simulated reflection coefficient characteristic reveals stop bands of 0.38 GHz (3.32–3.7 GHz) and 0.78 GHz (5.15 to 5.93 GHz) for $S_{11} \leq -10$ dB within the frequency span from 2.84 GHz to 13.36 GHz. The measured characteristic shows 0.52 GHz (3.19–3.7 GHz) and 0.87 GHz (5.05 to 5.92 GHz) stop bands which cover the entire WiMAX and WLAN band in frequency span of 2.88–13.71 GHz. The loss tangent of the substrate and dimensional mismatch between simulated and physical structures may cause the difference between the simulated and measured peak value at notch frequency.

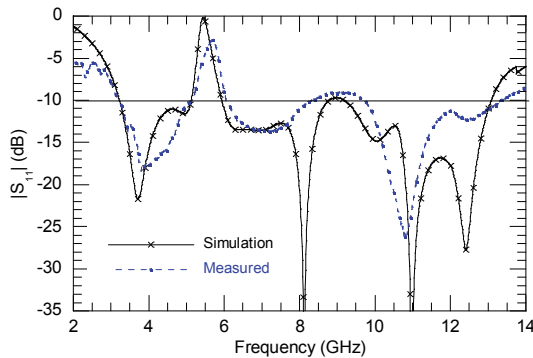


Fig. 18. Comparison between simulation and measured results of the prototype antenna with L-slots.

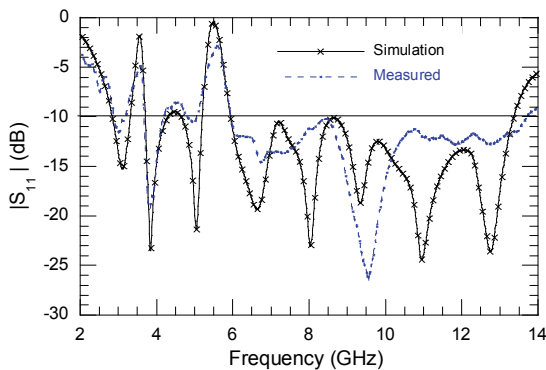


Fig. 19. Comparison between simulation and measured results of the proposed antenna.

5. Radiation Pattern

The radiation patterns are shown in Fig. 20. The antenna is printed in the X–Y plane and it is Y-polarized because the monopole is in the Y-direction. Therefore, the E-plane for this antenna is the YZ-plane and the H-plane is the XZ-plane.

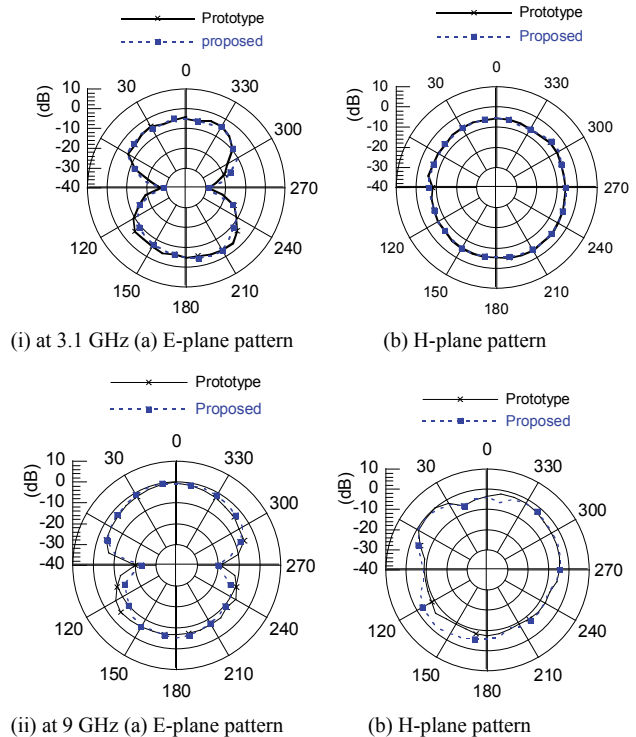


Fig. 20. Measured radiation pattern characteristics for the prototype (Fig. 16(a)) and the proposed antenna (Fig. 16(c, d)).

The H-plane radiation patterns are omnidirectional, whereas in E-plane, it is figure of eight because of small ground plane on the same side of the patch. It is to be noted that adding slots in the ground plane as well as strips on the other side substrate does not significantly alter the radiation patterns of the antenna. The results of Fig. 20 show that the radiation patterns are reasonably stable throughout ultra-wide band. Thus this can be considered as an UWB antenna with WiMAX, WLAN notch band characteristics for UWB applications.

6. Surface Currents and Input Impedance, Gain and Efficiency

Fig. 21 displays the current distribution of the proposed antenna. The current distribution at 3.1 GHz as shown in Fig. 21(a) indicates the excitation of lower order mode at this frequency.

The current distribution in Fig. 21(b) clearly indicates the formation of standing waves at notch frequency as the current is confined at the region of I-shape stubs. It is confirmed that the I-shape stubs effectively reflects the signal power back to the input port and thus mismatching occurs. As shown in Fig. 21(c), at another notch frequency, the current distribution is concentrated and oppositely directed on the interior and exterior sides of the slot. The current has high density at the edges of slot and low density at the corner point of the L-slot. The top of the slot is modeled as a transmission line short circuit mode. The resultant

equivalent load at the corner of the slot is high impedance (open circuit) due to the length from the top to the corner along the slot is approximately $\lambda/4$ at the notch frequency. Therefore, the slot behaves as an open-circuited load with large input impedance, causing a total impedance mismatch between the feed line and the radiating patch. As a result the desired notch band is created. The current distribution at 8 GHz as shown in Fig. 21(d) indicates the excitation of higher order mode at this frequency.

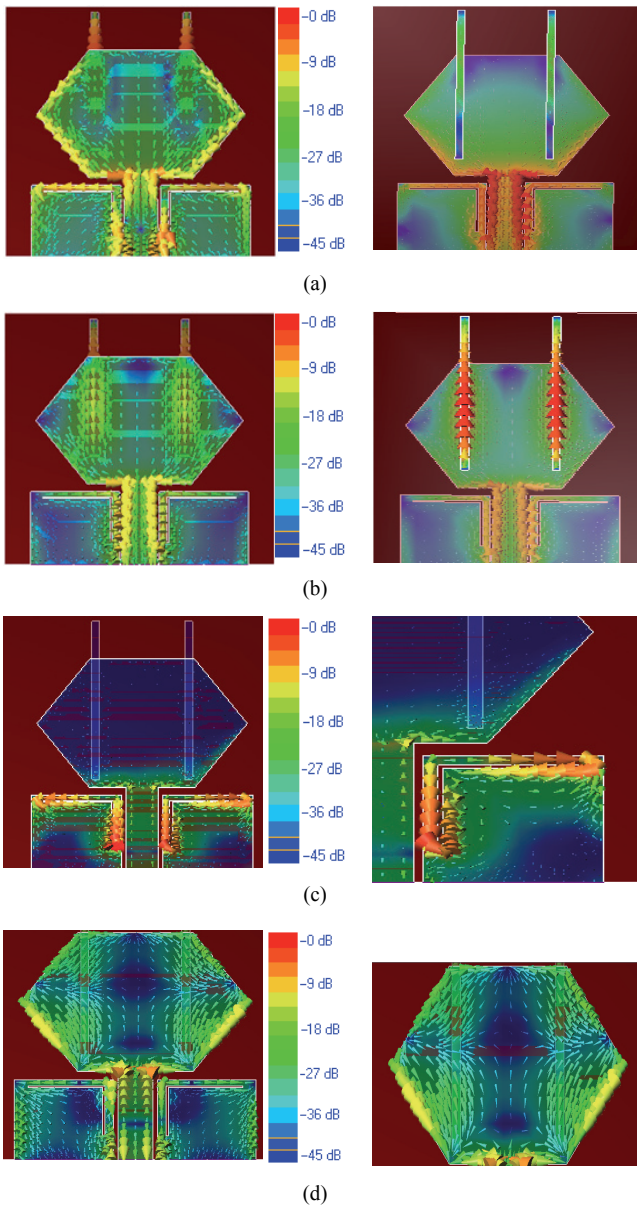


Fig. 21. Simulated current distribution at:(a) 3.1 GHz (left side - top plane; right side - bottom plane), (b) 3.5 GHz (left side - top plane; right side - bottom plane), (c) 5.5 GHz (left side -top plane; right side – zoomed of a slot) and (d) 8 GHz (left side –top plane; right side – zoomed of only patch).

The real and imaginary parts of the input impedance verses frequency of the prototype antenna is shown in Fig. 22. It is observed that the real part of the antenna im-

pedance varies around 50Ω while its imaginary part has small values and fluctuates around zero. This is mainly because of a continuous coupling obtained between the hexagonal patch and the ground plane and hence the matching is achieved over the entire UWB region. Fig. 23 shows the input impedance plot of the proposed antenna with notch frequencies. The impedance of the structure changes acutely at 3.5 GHz and 5.5 GHz as is evident from the very large value of its imaginary part. This causes large reflection at these frequencies resulting in steep rise of magnitude of S_{11} . In the notch bands, most of the power fed into the antenna is reflected back which leads to a decrease of the radiation efficiency and hence the antenna gain. The simulated gain is plotted in Fig. 24 in which two sharp drops occur at around 3.5 GHz and 5.5 GHz as expected. The similar variation can be seen in the antenna efficiency curve plotted in Fig. 25. This characteristic can make sure the ability of the proposed antenna to reject the

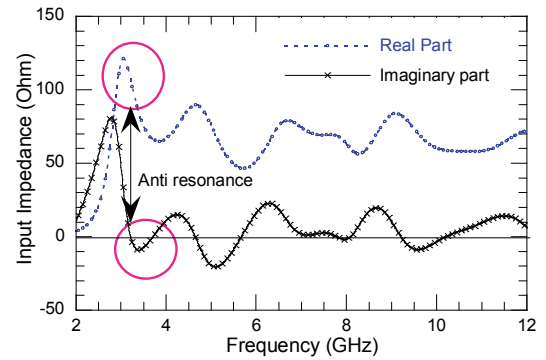


Fig. 22. Input impedance of the prototype antenna.

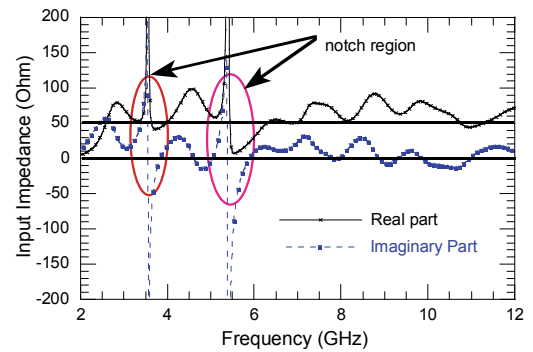


Fig. 23. Input impedance of the proposed antenna.

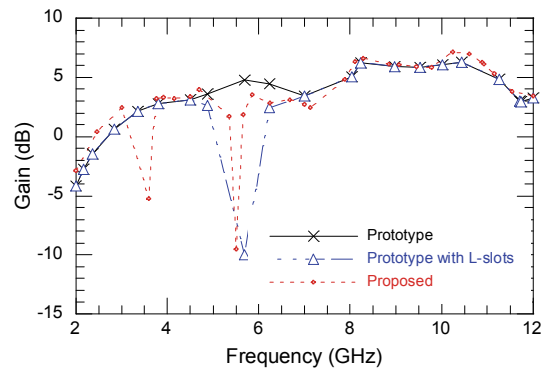


Fig. 24. Simulated gain versus frequency plot.

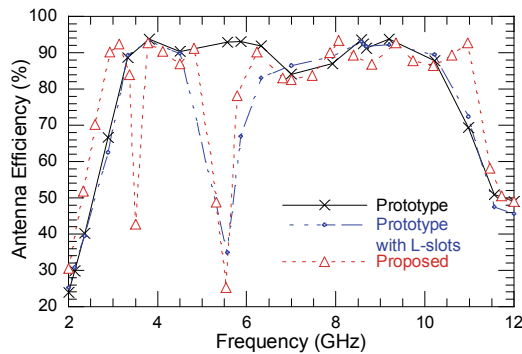


Fig. 25. Simulated antenna efficiency versus frequency plot.

interference effectively. The proposed antenna gain varies from 2.0 – 6.0 dB over the whole operating range except in notch bands. It provides antenna efficiency more than 80 % except at notch bands.

7. Transfer Function and Time Domain Study

A pair of proposed antennas is used as transmitting and receiving antenna to measure the magnitude of S_{21} and group delay. The transmitting and receiving antenna are placed at a distance of 170 mm. The measured magnitude of S_{21} and group delay of the proposed antenna are depicted in Fig. 26. The transfer function is relatively flat

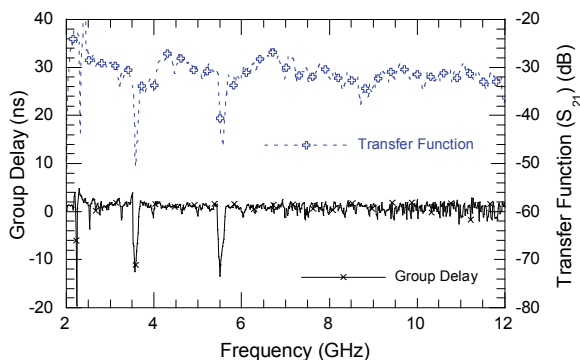


Fig. 26. The measured transfer function and group delay of the antenna systems (left side Y axis – Group delay; right side Y axis - S_{21}).

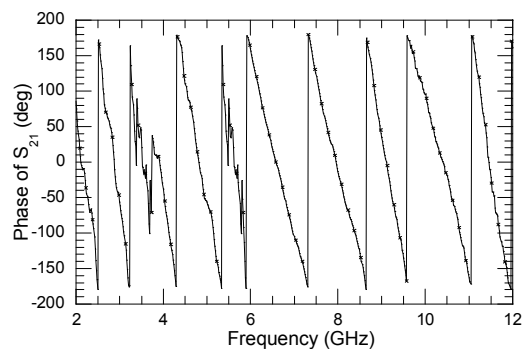


Fig. 27. The measured phase of S_{21} for the proposed antenna system.

(variation less than 10 dB) over the operating band except the notch bands. It is observed that the variation of group delay of the proposed antenna is virtually constant across the whole UWB band except at the two notch bands region. The measured phase of the transfer function is shown in Fig. 27. It is observed that the phase of S_{21} is relatively linear from 3 GHz to 12 GHz excluding the notch bands in face to face mode. The measured group delay corresponds well to the phase of S_{21} , so it proves that the antenna has a good time-domain characteristic and a small pulse distortion as well.

8. Conclusion

In this paper, a simple ultra-wideband planar hexagonal printed monopole antenna with dual narrow band-notch characteristics is presented. To realize the WLAN and WiMAX rejection bands in UWB, a couple of half wave length L-slots are added in the ground plane as well as a pair of I-shape strips placed on the other side of the patch. Input impedance, surface current distributions are built at the same time for analysis and explanation of dual narrow band-notch characteristics. The antenna has been successfully optimized, fabricated and measured. This antenna has ultra wide-band performance in the frequency band from 2.88 to 13.71 GHz for magnitude of $S_{11} \leq -10$ dB with dual excellent rejection bands. The radiation patterns are observed to be nearly omni-directional over the entire UWB frequency band. The proposed antenna peak gain varies between 2.0 dB and 6 dB at all frequencies other than the notch bands. Satisfactory time domain results have been found in respect of group delay and phase. Therefore the proposed antenna is expected to be a good candidate in various wireless applications.

References

- [1] First Report and Order, "Revision of part 15 of the commission's rule regarding ultra-wideband transmission system FCC 02- 48", *Federal Communications Commission*, 2002.
- [2] REZA GHADERI, M., MOHAJERI, F. A compact hexagonal wide slot antennas with microstrip fed monopole for UWB applications. *IEEE Antenna and Wireless Propagation Letters*, 2011, vol. 10, p. 682–685.
- [3] ZHANG, K., WANG, T., CHENG, L. L. Analysis of band notched UWB printed monopole antennas using a novel segmented structure. *Progress In Electromagnetics Research C*, 2013, vol. 34, p. 13–27.
- [4] MANDAL, T., DAS, S. Ultra wide band printed hexagonal monopole antennas with WLAN band rejection. *Microwave and Optical Technology Letters*, 2012, vol. 54, p. 1520–1525.
- [5] ABDO ABDEL MONEM SHAALAN, RAMADAN, M. I. Design of a compact hexagonal monopole antenna for ultra-wideband applications. *Journal of Infrared, Millimeter, and Terahertz Waves*, 2010, vol. 31, p. 958–96.
- [6] YI-CHENG LIN, KUAN-JUNG HUNG. Compact ultra-wide band rectangular aperture antenna and band-notched designs. *IEEE*

- Transactions on Antennas and Propagation*, 2006, vol. 54, no. 11, p. 3075-3081.
- [7] LIANG, J., GUO, L., CHIAU, C. C., CHEN, X., PARINI, C.G. Study of CPW-fed circular disc monopole antenna. *IEE Proceedings on Microwaves, Antennas and Propagation*, 2005, vol. 152, no. 6, p. 520–526. doi:10.1049/ip-map:20045179.
- [8] HABIB, M. A., BOSTANI DJAIZ, A., NEDIL, M., YAGOUB, M. C. E., DENIDNI, T. A. Ultra wideband CPW-fed aperture antenna with WLAN band rejection. *Progress In Electromagnetics Research*, 2010, vol. 106, p. 17–31.
- [9] PENGCHENG LI, JIANXIN LIANG, XIAODONG CHEN. Study of printed elliptical/circular slot antennas for ultra-wide band applications. *IEEE Transactions on Antennas and Propagation*, 2006, vol. 54, no. 6, p. 1670–1675.
- [10] RAY, K. P., TIWARI, S. Ultra wide band printed hexagonal monopole antennas. *IET Microwaves, Antennas and Propagation*, 2010, vol. 4, no. 4, p. 437–445. DOI: 10.1049/iet-map.2008.0201.
- [11] GHATAK, R., BISWAS, B., KARMAKAR, A., PODDAR, D. R. A circular fractal UWB antenna based on Descartes circle theorem with band rejection capability. *Progress In Electromagnetics Research C*, 2013, vol. 37, p. 235–248.
- [12] SUN, A., YIN, Y. Z., JING, S. H., YANG, Y., LIU, B. W., LI, Z. Broadband CPW-fed antenna with band-rejected characteristics for WLAN/WiMAX operation. *Progress In Electromagnetics Research C*, 2011, vol. 22, p. 47–54.
- [13] ZHOU, D., GAO, S., ZHU, F., ABD – ALHAMEED, R. A., XU, J. D. A simple and compact planar ultra wide-band antenna with single or dual band notched characteristics. *Progress In Electromagnetic Research C*, 2012, vol. 123, p. 47–65.
- [14] FEI YU, CHUNHUA WANG. A CPW-fed novel planar ultra-wideband antenna with a band-notch characteristic. *Radioengineering*, 2009, vol. 18, no. 4, p. 551–555.
- [15] MANDAL, T., DAS, S. Design and analysis of a coplanar waveguide fed ultra wideband hexagonal open slot antenna with WLAN and WiMAX band rejection. *Microwave and Optical Technology Letter*, 2014, vol. 56, no. 2, p. 434–443.
- [16] CHATTOPADHYAY, K., DAS, S., DAS, S., BHADRA CHAUDHURI, S. R. Ultra-wideband performance of printed hexagonal wide slot antenna with dual band-notched characteristics. *Progress In Electromagnetics Research C*, 2013, vol. 44, p. 83–93.
- [17] MA, X. L., SHAO, W., HE, G. Q. A novel dual narrow band-notch band CPW fed UWB slot antenna with parasitic strips. *Applied Computational Electromagnetic Society*, 2012, vol. 27, no. 7, p. 581–588.
- [18] KIM, K. H., PARK, S. O. Analysis of the small band rejected antenna with the parasitic strip for UWB. *IEEE Transactions on Antennas and Propagation*, 2006, vol. 54, no. 6, p. 1688–1692.
- [19] KIM, D. O., JO, N. I., JANG, H. A., KIM, C. Y. Design of the ultra wide band antenna with a quadruple-band rejection characteristics using a combination of the complementary split ring resonators. *Progress In Electromagnetic Research*, 2011, vol. 112, p. 93–107.
- [20] ISLAM, M.T., AZIM, R., MOBASHSHER, A. T. Triple band notched planar UWB antenna using parasitic strips. *Progress In Electromagnetic Research*, 2012, vol. 129, p. 161–179.
- [21] YINGSONG LI, WENXING LI, TAO JIANG. Implementation and investigation of a compact circular wide slot UWB antenna with dual notched band characteristics using stepped impedance resonators. *Radioengineering*, 2012 vol. 21, no.1, p. 517–527.
- [22] Zeland IE3D™ software.

About Authors...

Tapan MANDAL (1977) received the B. Tech. degree in Electronics and Communication Engineering from Kalyani Govt. Engineering College of Kalyani University in 2001. He has done M.E. Degree from Bengal Engineering College (D.U.), Shibpur India, in 2003. From 2004 to 2007, he worked as a Lecturer at the University Institute of Technology, Burdwan University. Since 2007, he is associated with the Department of Information Technology of Govt. College of Engineering and Textile Technology, Serampore, India and presently holds the post of an Asst. Professor. His current research interests include the planar printed antenna and electromagnetic band gap structures.

Santanu DAS (1968) received the B. E. degree in Electronics and Telecommunication Engineering from Bengal Engineering College of Calcutta University (India) in 1989 and M.E. degree in Microwave Engineering from Jadavpur University, Calcutta, in 1992. He obtained the Ph.D. (Engineering) degree from Jadavpur University in 1998. He joined the Department of Bengal Engineering and Science University, India in the year 1998, as a Lecturer in the Electronics and Telecommunication Engineering and presently holds the post of Professor. His current research interests include microstrip circuits, FSS, antenna elements and arrays. He is a life member of the Institution of Engineers, India.